

OPTIMIZATION OF BODY CONFIGURATION AND JOINT-DRIVEN ATTITUDE STABILIZATION FOR TRANSFORMABLE SPACECRAFTS UNDER SOLAR RADIATION PRESSURE

A PREPRINT

 **Yuki Kubo**

Institute of Space and Astronautical Science
Japan Aerospace Exploration Agency
Sagamihara, 252-5210, Japan
kubo.yuki@jaxa.jp

 **Toshihiro Chujo**

Department of Mechanical Engineering
Tokyo Institute of Technology
Ookayama, 152-8550, Japan
chujo.t.aa@m.titech.ac.jp

May 19, 2023

ABSTRACT

A solar sail is one of the most promising space exploration system because of its theoretically infinite specific impulse using solar radiation pressure (SRP). Recently, some researchers proposed "transformable spacecrafts" that can actively reconfigure their body configurations with actuatable joints. The transformable spacecrafts are expected to greatly enhance orbit and attitude control capability due to its high redundancy in control degree of freedom if they are used like solar sails. However, its large number of input poses difficulties in control, and therefore, previous researchers imposed strong constraints to limit its potential control capabilities. This paper addresses novel attitude control techniques for the transformable spacecrafts under SRP. The authors have constructed two proposed methods; one of those is a joint angle optimization to acquire arbitrary SRP force and torque, and the other is a momentum damping control driven by joint angle actuation. Our proposed methods are formulated in general forms and applicable to any transformable spacecraft that has front faces that can dominantly receive SRP on each body. Validity of the proposed methods are confirmed by numerical simulations. This paper contributes to making most of the high control redundancy of transformable spacecrafts without consuming any expendable propellants, which is expected to greatly enhance orbit and attitude control capability.

Keywords Solar sail · Transformable spacecraft · Attitude–joint coupled motion · Attitude stabilization

Nomenclature

CoM	center of mass
SRP	solar radiation pressure
θ_k	angular displacement of the k -th actuatable joint (rad)
$\theta (= [\theta_1, \dots, \theta_m]^T)$	joint angle vector (rad)
λ_k	rotational axis of the k -th joint
ω	angular velocity of body 0 (rad/s)
R_X	absolute position of the CoM of body X (m)
$r_{XY} (= R_X - R_Y)$	relative position of the CoM of X with respect to the CoM of Y (m)
$r_X (= R_X - R_0)$	relative position of the CoM of X with respect to the CoM of body 0 (m)
h_c	angular momentum around the CoM of whole bodies ($\text{kg} \cdot \text{m}^2/\text{s}$)
I_X	moment of inertia of X around the CoM of the X ($\text{kg} \cdot \text{m}^2$)
m_X	total mass of X (kg)
M	generalized mass matrix
v	generalized velocity
w	generalized acceleration
d	second-order term of a generalized velocity
τ	generalized force
U	identity matrix
x^\times	skew symmetric matrix of a vector $x \in \mathbb{R}^3$
$(\cdot)_k$	subscript which signifies the k -th body
$(\cdot)_c$	subscript which signifies the whole bodies
$(\cdot)_{\hat{k}}$	subscript which signifies the k -th outer group
$(\cdot)_{h_k}$	subscript which signifies the k -th joint
$(\cdot)_{s_{ij}}$	subscript which signifies the j -th surface of the i -th body
$\phi (= [\phi_1, \phi_2, \phi_3]^T)$	Euler angles (rad)
C	direction cosine matrix
t	time (s)
s	sun pointing vector
n_i	normal vector of i -th body
P	solar radiation pressure (SRP) (Pa)
F	SRP force (N)
T	SRP torque ($\text{N} \cdot \text{m}$)
$C_{\text{spe}}, C_{\text{dif}}, C_{\text{abs}}$	coefficient of optical properties
Q, R	weight matrices for LQR feedback control

1 Introduction

1.1 Background

Solar radiation pressure (SRP) is a potential propulsion resource in inter-planetary space missions, and its active use for space flight has been investigated for a long time. In particular, a solar sail, which has large and thin membrane structure, is promising as a propellant-free propulsion system using SRP, and has been investigated by a lot of researchers [1, 2, 3, 4, 5, 6, 7, 8]. A solar sail controls its orbit by maneuvering attitude with respect to the sun, and therefore its attitude control method has crucial impacts on its orbit control capability. Attitude control methods of solar sails are classified into major two types depending on their membrane deployment systems: 1) spin-type, 2) boom-type. The former type deploys its membrane by centrifugal force of spinning motion without any stiff structures, which was demonstrated by IKAROS [9, 10]. The spin-type is preferable for large-size sail in terms of mass and besides, can naturally stabilize its attitude by rotational stiffness. However, it requires more time and energy to change its attitude and cannot slew its orientation flexibly and agilely. In contrast, the boom-type uses stiff support structure to maintain the shape of its membrane and usually adopts three-axis attitude stabilization with actuators such as magnetorquers and reaction wheels [11]. However, attitude stabilization of large membrane requires very large torque because its moment of inertia increases in proportional to r^4 where r is a radius of the membrane. Moreover, neither of both types can orient its spacecraft bus independently of the membrane, and thus limits permissible attitude of the sail due to orientation constraints imposed on bus components such as antennas, cameras, and thrusters. All of the above problems restricts orbit control capability of solar sails.

As promising solutions to these problems, some researchers have been proposing novel solar sailing techniques in which the shape of the membrane is dynamically and independently controlled. Takao [12, 13, 14] has proposed active shape control of sail membrane for spin-type solar sails. The main concept is to excite resonant oscillation on the membrane surface synchronized with its spin frequency, so that the shape of the membrane is actively changed seen from inertial frame. This technique enables the orientation of membrane and a spacecraft bus to be independently controlled and contributes to enhancing orbit control capability. However, the nonlinear dynamics of the dynamically oscillated membrane causes a lot of difficulties in control. In addition, achievable orientation of the membrane is constrained by magnitude of excitable oscillation.

Another promising solution is to add active joints to a solar sail, which is referred to as a transformable solar sail. The actuatable joints enable relative geometry of sail membranes dynamically reconfigurable, and thus can contribute to satisfying orientation constraints of instruments while SRP torque and force are properly controlled to obtain desired attitude and orbit. Moreover, the transformable solar sail can carry out propellant-free attitude reorientation enabled by nonholonomic properties of attitude equations of free-floating multi-bodies [15, 16, 17, 18, 19, 20, 21]. Chujo [22] formulated attitude motion of solar sails with variable-shape mechanisms in which large deformation of body components is properly handled without approximations. In addition, Chujo carried out stability analysis and propellant-free attitude maneuver for a specific spacecraft with four actuatable paddles. Another example is Abrishami and S. Gong's work [23] that proposed a redundant control method for a solar sail with four actuatable petals equipped with reflectivity control devices (RCD). They solved a complex mixed-integer-continuous and nonlinear optimization problem by approximating SRP torque with a modified egg-shaped equation. However, a degree of freedom of actuatable joints is limited to 2–4 in most transformable solar sails because flexible membrane structure cannot mechanically hold heavy joint mechanisms on it. This mechanical constraint makes it difficult for transformable solar sails to simultaneously satisfy orientation constraints of multiple instruments. In addition, most formulations have not dealt with attitude-joint coupled dynamics. Chujo's work [22] and Abrishami's work [23] have not considered dynamic joint actuation during solar sailing and H. Gong's work [24] has not included effect of SRP torque in its attitude control. However, it is crucial to derive such a control law that properly handles attitude-joint coupled dynamics to make the most of transformable solar sails.

Recently, another novel and promising spacecraft, a transformable spacecraft is investigated by several researchers including the authors [25, 26]. The transformable spacecraft is composed of multiple rigid body components connected with electrically actuatable joints and can reconfigure geometry of body components dynamically. Unlike the transformable solar sail, the transformable spacecraft can install a lot of actuatable joints on rigid body components. Thus, the highly redundant degree-of-freedom in control enables it to satisfy orientation constraints of multiple instruments, and besides, to carry out more agile nonholonomic attitude reorientation maneuver. However, control strategy of previous works largely depend on the simplicity (and in most case, symmetricity) of specific models of transformable spacecrafts. Chujo's another work proposed a control strategy with a highly redundant transformable spacecraft, but it sacrificed most of the control degree of freedom to simplify the problem of attitude and body configuration optimization under SRP [27]. Thus, attitude control strategy of transformable spacecrafts with large number of active joints has not generally been derived. Moreover, attitude-joint coupled dynamics have not been solved to plan attitude maneuver as is the case with the transformable solar sails [22, 23, 24].

1.2 Contributions

In this paper, we propose an attitude-joint coupled control method that can be applicable to arbitrary transformable spacecrafts under SRP exposure. Our contribution is divided into two novel techniques: 1) joint angle optimization to satisfy arbitrary SRP force and torque constraints (*SRP-based joint angle optimization*), 2) angular momentum damping control by attitude-joint coupled control. The former method contributes to obtaining neutrally stable equilibrium attitude and body configuration under SRP field to acquire arbitrary SRP acceleration. Unlike the previous method [27], our technique can handle general body configurations without restricting the control degree of freedom, and thus greatly enhances solar sailing capability of transformable spacecrafts. The latter technique, the angular momentum damping control, contributes to asymptotically stabilizing the equilibrium attitude obtained by the above joint angle optimization technique. We formulated a generalized attitude motion that can handle attitude-joint coupled motion to obtain the control law. This technique can also be applicable to arbitrary transformable spacecraft and does not require any other additional actuators such as reaction wheels and reflectivity control devices.

1.3 Organization of the paper

Section 2 provides preliminary formulations to prepare for the following sections. Section 3 formulates the two novel proposed techniques: joint angle optimization and angular momentum damping control. Section 4 describes setups of

numerical simulations and shows their result. Section 5 summarizes the contents of the present paper and provides concluding remarks.

2 Preliminary formulations

This section provides some preliminary formulations for the following sections. Nomenclature used in the following formulations is listed in the beginning of this paper. Throughout this paper, we clearly distinguish a vector and its component; a mathematical symbol with bold font stands for a vector entity, and that with a normal font stands for a component matrix of the vector expressed with a certain set of reference basis vectors. For example, dot-product and cross-product operations are defined for vectors as $(\mathbf{x} \cdot \mathbf{y})$ and $\mathbf{x} \times \mathbf{y}$ respectively while the same operations are expressed with $(x^T y)$ and $(x \times y)$ for vector components. In addition, all vector components are expressed in body frame unless their reference frame is explicitly indicated.

2.1 Attitude dynamics of free-flying multi bodies

The formulation of this section largely follows the author's previous work [28]. The nomenclature for body components and their relationship are shown in Fig. 1. The characters defined in this figure can be interpreted with the nomenclature list at the beginning of this paper. R_k , R_0 and R_c represent the absolute position of the CoM of k -th body, 0-th body and whole bodies respectively, whereas r_k expresses the relative position of the CoM of the k -th body with respect to the CoM of body 0. In this representation, an entire spacecraft is divided into a main body that is assigned an index $k = 0$, and some other branches growing from the main body. Here, for convenience of formulation, we assume that each branch has no loop structure. This assumption assures serial index assignment from the main body (innermost, root) to the tip of each branch (outermost, tips). Body indices in each branch are allotted sequentially from an inner body to an adjacent outer body. The hinge joint component connecting the k -th body and its inside neighbor is labeled a k -th joint, and a set of all bodies outside of the k -th joint are labeled \hat{k} , which is referred to as k -th outer group. Note that all indices in the outer group \hat{k} are larger than k from the above definitions. This \hat{k} grouping contributes to simple formulations because all bodies in the k -th outer group move in the same manner when the k -th joint is actuated. The rotational degree of freedom of each hinge joint is set to be 1, and the rotational angle of the k -th joint is described as θ_k . Any joint rotation can be expressed by a combination of 1-dimensional rotations, and hence this assumption does not lose generality. The body frame is attached to the main body ($k = 0$), and its origin is at the center of mass (CoM) of the main body. Thus, the attitude of the entire multi body system is represented by the attitude of the main body hereafter. Note that the position of the CoM for the entire spacecraft is not fixed in the body-fixed coordinate as the spacecraft changes its body configuration.

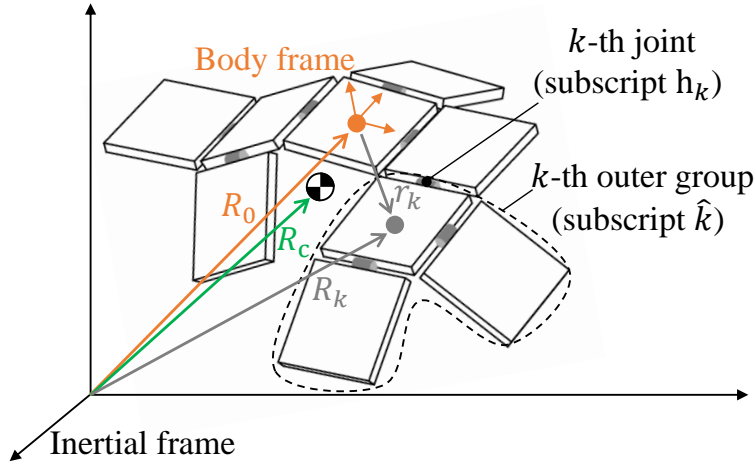


Figure 1: Nomenclature for body components and their positions

We use the Kane's formulation in the present paper, which generally contributes to rapid numerical computation [29, 30]. A general form of the dynamics equation can be described as follows:

$$\begin{bmatrix} M_{vv} & M_{v\omega} & M_{v\theta} \\ M_{\omega v} & M_{\omega\omega} & M_{\omega\theta} \\ M_{\theta v} & M_{\theta\omega} & M_{\theta\theta} \end{bmatrix} \begin{bmatrix} w_v \\ w_\omega \\ w_\theta \end{bmatrix} + \begin{bmatrix} d_v \\ d_\omega \\ d_\theta \end{bmatrix} = \begin{bmatrix} \tau_v \\ \tau_\omega \\ \tau_\theta \end{bmatrix} \quad (1)$$

or for short,

$$Mw + d = \tau \quad (2)$$

where M , w , d and τ are a generalized mass matrix, a generalized acceleration, a second order term of a generalized velocity and generalized force respectively. In addition, the subscripts $(\cdot)_v$, $(\cdot)_\omega$ and $(\cdot)_\theta$ indicate translational velocity, rotational velocity and joint speed respectively. The corresponding generalized velocities are the translational velocity of the CoM of the entire spacecraft v_v , the angular velocity of the main body v_ω , and the joint actuation speed v_θ , which are all expressed in the body frame:

$$v_v = v_c = \begin{bmatrix} v_{c,x} \\ v_{c,y} \\ v_{c,z} \end{bmatrix} \in \mathbb{R}^3 \quad v_\omega = \omega = \begin{bmatrix} \omega_x \\ \omega_y \\ \omega_z \end{bmatrix} \in \mathbb{R}^3 \quad v_\theta = \dot{\theta} = \begin{bmatrix} \dot{\theta}_1 \\ \vdots \\ \dot{\theta}_m \end{bmatrix} \in \mathbb{R}^m \quad (3)$$

where m is the number of hinge joints of a transformable spacecraft. An explicit description of the components in Eq. (1) is given in Appendix A. The important point is that the terms $M_{v\omega}$, $M_{v\theta}$, $M_{\omega v}$, and $M_{\theta v}$ are all zero in this expression, which means translational and rotational motions are not coupled and independently solved. In this paper, our interest is on attitude motion, and therefore the first row of Eq. (1) does not appear in the following discussions. In addition, this paper assumes that control input of the system is given as joint acceleration w_θ and required joint torque τ_θ is ideally provided to realize the desired joint acceleration. Therefore, the fundamental equation handled in this paper is the second row of Eq. (1):

$$\begin{aligned} M_{\omega\omega}w_\omega + M_{\omega\theta}w_\theta + d_\omega &= \tau_\omega \\ \leftrightarrow M_{\omega\omega}\dot{w}_\omega + M_{\omega\theta}\ddot{\theta} + d_\omega &= \tau_\omega \end{aligned} \quad (4)$$

Moreover, the total angular momentum h_c around the centroid of the entire spacecraft can be represented as follows:

$$h_c = M_{\omega\omega}v_\omega + M_{\omega\theta}v_\theta = M_{\omega\omega}\omega + M_{\omega\theta}\dot{\theta} \quad (5)$$

The first term is angular momentum of rotation of an entire spacecraft and the second term is angular momentum of relative rotation of body components.

2.2 Formulation of solar radiation pressure

Solar radiation pressure (SRP) is pressure applied on a sunlit surface. Current standard formulation decomposes the SRP into three major factors: specular, diffusion, and absorption [31]. Each factor is illustrated in Fig. 2.

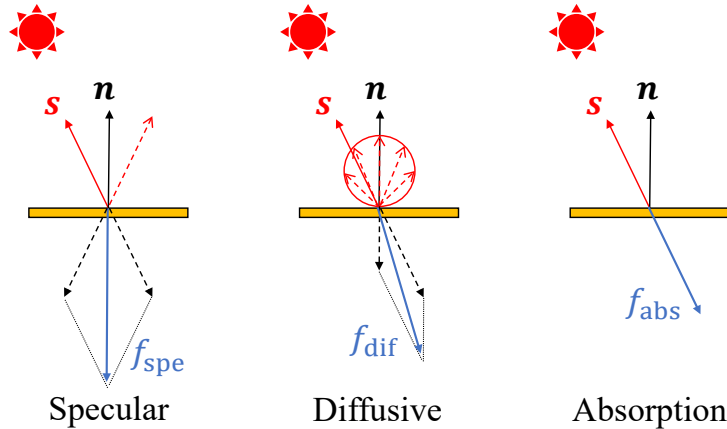


Figure 2: Three factors for SRP force (from left): specular, diffusive, absorptive

In this paper, we set an assumption that the transformable spacecraft is composed only of flat surfaces. Under this assumption, the SRP force exerted on a j -th surface of an i -th body is characterized by the area of the surface, direction of its (outward-pointing) normal vector and its optical properties as:

$$\begin{aligned}
F_{ij} &= \begin{cases} \hat{F}_{ij} & (n_{ij}^\top s \geq 0) \\ 0 & (n_{ij}^\top s < 0) \end{cases} \\
\hat{F}_{ij}(s, n_{ij}) &= -PA_{ij}(n_{ij}^\top s) \{ (C_{absij} + C_{difij})s \\
&\quad + \left(\frac{2}{3}C_{difij} + 2(n_{ij}^\top s)C_{speij} \right) n_{ij} \} \\
&= -(p_{n1ij}n_{1ij} + p_{n2ij}n_{2ij} + p_{sij}s_{ij})A_{ij} \\
\text{where } p_{n1ij} &= 2PC_{speij}, \quad p_{n2ij} = \frac{2}{3}PC_{difij}, \quad p_{sij} = P(C_{absij} + C_{difij}), \\
n_{1ij} &= (n_{ij}^\top s)^2 n_{ij}, \quad n_{2ij} = (n_{ij}^\top s)n_{ij}, \quad s_{ij} = (n_{ij}^\top s)s
\end{aligned} \tag{6}$$

As the first equation indicates, SRP force is exerted on the surface where its normal vector is directed to the sun. Note that the shadow detection computing is not performed in this paper due to limited computational resource. C_{speij} , C_{difij} , and C_{absij} are respectively coefficients for the specularly, diffusion, and absorption of the j -th surface of the i -th body that holds $C_{speij} + C_{difij} + C_{absij} = 1$. A_{ij} is an area of the j -th surface of the i -th body. $s \in \mathbb{R}^3$ and $n_{ij} \in \mathbb{R}^3$ are components of the vectors towards the sun from the surface and the normal vector of the j -th surface of the i -th body respectively (both are unit vectors). P is the solar radiation pressure applied on a certain surface expressed as follows:

$$P = \frac{S_0}{c} \left(\frac{1}{\text{AU}} \right)^2 \tag{7}$$

where S_0 , c , AU are a solar constant, a speed of light, and a distance between the sun and a spacecraft expressed in an astronomical unit. Total force and torque applied on a spacecraft are:

$$\begin{aligned}
F &= \sum_i \sum_j F_{ij} \\
T &= \sum_i \sum_j T_{ij} = \sum_i \sum_j (r_{s_{ij}i} + r_{ic})^\times F_{ij} = \sum_i \sum_j (R_{s_{ij}} - R_c)^\times F_{ij}
\end{aligned} \tag{8}$$

Again, the characters appearing in this equation can be interpreted with the nomenclature list at the beginning of this paper. $r_{s_{ij}i}$ is the relative position of the center of the j -th surface of the i -th body with respect to the CoM of the i -th body, r_{ic} is the relative position of the CoM of the i -th body with respect to the CoM of an entire spacecraft. x^\times is a skew symmetric matrix of a component vector $x \in \mathbb{R}^3$.

2.3 Jacobian of SRP torque

Difference of SRP torque is important for analytical discussions and designing stabilization controls. This section is devoted to derivation of the Jacobian. The SRP torque applied on a spacecraft is dependent on attitude and joint angles. Thus, its total derivative is expressed as:

$$dT = \frac{\partial T}{\partial \phi} d\phi + \frac{\partial T}{\partial \theta} d\theta \tag{9}$$

where attitude is expressed with Euler angles $\phi = [\phi_1, \phi_2, \phi_3]$. The following analysis can be applied to any Euler sequence, but 2-1-3 sequence is adopted in this paper. The relationships of the coordinate are shown in Fig. 3. Components of sun-direction vector expressed in body fixed frame is:

$$s = \begin{bmatrix} \cos \phi_1 \sin \phi_2 \sin \phi_3 - \sin \phi_1 \cos \phi_3 \\ \cos \phi_1 \sin \phi_2 \cos \phi_3 + \sin \phi_1 \sin \phi_3 \\ \cos \phi_1 \cos \phi_2 \end{bmatrix} \tag{10}$$

Jacobians of n_{2ij} and s_{ij} are discontinuous at $n_{ij}^\top s = 0$. To avoid this discontinuity when calculating control input, we set two assumptions. First, we assume all body components have a front face to receive SRP dominantly. This assumption is valid in most cases because a transformable spacecraft should consist of panel-like structures if it is designed to effectively use SRP and to compactly be stowed on a launch vehicle. Second, it is assumed that the front face always satisfies $n_{ij}^\top s > 0$ during a simulation. This assumption is also valid in most cases because the proposed

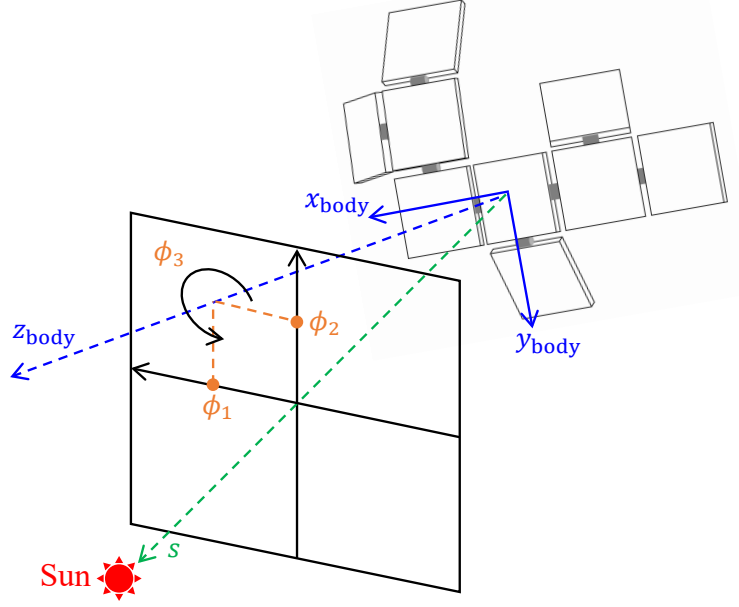


Figure 3: Definitions of coordinate related to attitude motion

control law can be effective when a spacecraft have small and slow attitude oscillation around a sun-facing nominal attitude. These assumptions can prevent the Jacobian from being discontinuous, but rather generate modeling error of SRP. Validity of the control law under this modeling error is confirmed in Section 4. Hereafter, the n_{1ij} , n_{2ij} and s_{ij} of the front face are denoted as n_{1i} , n_{2i} and s_i . Under these assumptions, Jacobian of n_{1i} , n_{2i} , s_i with respect to Euler angles ϕ are expressed as follows:

$$\begin{aligned}
 \frac{\partial n_{1i}}{\partial \phi_j} &= 2(n_i^\top s) \left(n_i^\top \frac{\partial s}{\partial \phi_j} \right) n_i \\
 \frac{\partial n_{2i}}{\partial \phi_j} &= \left(n_i^\top \frac{\partial s}{\partial \phi_j} \right) n_i \\
 \frac{\partial s_i}{\partial \phi_j} &= \left(n_i^\top \frac{\partial s}{\partial \phi_j} \right) s + (n_i^\top s) \frac{\partial s}{\partial \phi_j} \\
 \frac{\partial s}{\partial \phi_1} &= \begin{bmatrix} -\sin \phi_1 \sin \phi_2 \sin \phi_3 - \cos \phi_1 \cos \phi_3 \\ -\sin \phi_1 \sin \phi_2 \cos \phi_3 + \cos \phi_1 \sin \phi_3 \\ -\sin \phi_1 \cos \phi_2 \end{bmatrix} \\
 \frac{\partial s}{\partial \phi_2} &= \begin{bmatrix} \cos \phi_1 \cos \phi_2 \sin \phi_3 \\ \cos \phi_1 \cos \phi_2 \cos \phi_3 \\ -\cos \phi_1 \sin \phi_2 \end{bmatrix} \\
 \frac{\partial s}{\partial \phi_3} &= \begin{bmatrix} \cos \phi_1 \sin \phi_2 \cos \phi_3 + \sin \phi_1 \sin \phi_3 \\ -\cos \phi_1 \sin \phi_2 \sin \phi_3 + \sin \phi_1 \cos \phi_3 \\ 0 \end{bmatrix}
 \end{aligned} \tag{11}$$

where $\frac{\partial X}{\partial \phi_j}$ indicates j -th column of $\frac{\partial X}{\partial \phi}$. Jacobian of SRP torque with respect to Euler angles is provided as:

$$\begin{aligned}
 \frac{\partial T}{\partial \phi_j} &= \sum_i (R_{s_i} - R_c) \times \frac{\partial F_i}{\partial \phi_j} \\
 \text{where } \frac{\partial F_i}{\partial \phi_j} &= - \left(p_{n1i} \frac{\partial n_{1i}}{\partial \phi_j} + p_{n2i} \frac{\partial n_{2i}}{\partial \phi_j} + p_{s_i} \frac{\partial s_i}{\partial \phi_j} \right) A_i
 \end{aligned} \tag{12}$$

where F_{ij} , $R_{s_{ij}}$ and A_{ij} of the front face are denoted as F_i , R_{s_i} and A_i . On the other hand, Jacobian with respect to joint angles can be computed with the following procedure. Derivative of torque on i -th body with respect to angular

displacement of k -th joint is:

$$\frac{\partial T_i}{\partial \theta_k} = \left(\frac{\partial R_{s_i}}{\partial \theta_k} - \frac{\partial R_c}{\partial \theta_k} \right)^\times F_i + (R_{s_i} - R_c)^\times \frac{\partial F_i}{\partial n_i} \frac{\partial n_i}{\partial \theta_k} \quad (13)$$

The difference of CoM positions, $\frac{\partial R_c}{\partial \theta_k}$ and $\frac{\partial R_i}{\partial \theta_k}$ are expressed as:

$$\begin{aligned} \frac{\partial R_c}{\partial \theta_k} &= \frac{\hat{m}_k}{m} \lambda_k^\times r_{\hat{k}h_k} \\ \frac{\partial R_{s_i}}{\partial \theta_k} &= \begin{cases} \lambda_k^\times r_{s_i h_k} & (i \in \hat{k}) \\ 0 & (i \notin \hat{k}) \end{cases} \end{aligned} \quad (14)$$

Derivative of SRP force with respect to difference of i -th normal vector is:

$$\begin{aligned} \frac{\partial F_i}{\partial n_i} &= -PA_i \left\{ (C_{abs_i} + C_{dif_i})s + \left(\frac{2}{3}C_{dif_i} + 2(n_i^\top s)C_{spe_i} \right) n_i \right\} s^\top \\ &\quad - PA_i (n_i^\top s) \left\{ 2C_{spe_i} n_i s^\top + \left(\frac{2}{3}C_{dif_i} + 2(n_i^\top s)C_{spe_i} \right) U \right\} \\ &= -PA_i \left\{ (C_{abs_i} + C_{dif_i})ss^\top + \left(\frac{2}{3}C_{dif_i} + 4(n_i^\top s)C_{spe_i} \right) n_i s^\top \right. \\ &\quad \left. + (n_i^\top s) \left(\frac{2}{3}C_{dif_i} + 2(n_i^\top s)C_{spe_i} \right) U \right\} \end{aligned} \quad (15)$$

The last term, difference of normal vector of i -th body with respect to angular displacement of k -th joint is:

$$\frac{\partial n_i}{\partial \theta_k} = \begin{cases} \lambda_k^\times n_i & (i \in \hat{k}) \\ 0 & (i \notin \hat{k}) \end{cases} \quad (16)$$

The derivative of torque on i -th body with respect to k -th joint actuation can be computed by substituting Eqs. (14)–(16) into Eq. (13). Finally, the total derivative of the SRP torque on an entire spacecraft is obtained by substituting Eqs. (12) and (13) into Eq. (9).

3 Proposed methods

3.1 SRP-based joint angle optimization

This section describes an optimization problem to obtain optimal attitude and joint angles that satisfies target SRP force and torque while achieving stable attitude motion. The optimization problem is defined as follows:

$$\begin{aligned} &\underset{\phi, \theta}{\text{minimize}} && f(\phi, \theta) \\ &\text{subject to} && c(\phi, \theta) \leq 0, \quad c_{\text{eq}}(\phi, \theta, F_{\text{targ}}, T_{\text{targ}}) = 0, \quad \theta_{\text{lb}} \leq \theta \leq \theta_{\text{ub}} \end{aligned} \quad (17)$$

where $\theta_{\text{lb}}, \theta_{\text{ub}} \in \mathbb{R}^m$ are lower and upper bound of joint angles. Each function in the above optimization problem is set as follows:

$$\begin{aligned} f &= -\left\| \text{Im}(\sqrt{\Lambda}) \right\|_\infty \\ c &= \max(\text{Re}(\sqrt{\Lambda})) \\ c_{\text{eq}} &= \begin{bmatrix} F_{\text{targ}} - F \\ T_{\text{targ}} - T \end{bmatrix} \end{aligned} \quad (18)$$

where $\|\cdot\|_\infty$ is an L-infinity norm of vector components, $\text{Re}(\cdot)$ and $\text{Im}(\cdot)$ take real and imaginary part of each component respectively, and $\max(\cdot)$ takes a maximum value of all of the components. Λ is a 3×1 matrix that contains all three eigenvalues of the following matrix $A_\phi \in \mathbb{R}^{3 \times 3}$:

$$A_\phi = C_\phi I_c^{-1} \frac{\partial T}{\partial \phi} \quad (19)$$

where C_ϕ is a matrix that converts angular velocity into Euler angle velocity, hence $\dot{\phi} = C_\phi \omega$. The objective function f evaluates frequency of attitude oscillation. The time scale of this frequency determines time scale of the damping control described later in Section 3.2, and therefore it is minimized to attain rapid momentum damping. The nonlinear inequality constraint c determines divergence property of the attitude motion, where $c \leq 0$ means the attitude motion does not diverge. Actually, it is shown by Chujo that c does not become negative under SRP torque field [22]. However, we rather set $c \leq 0$ because the convergence performance of the solver is improved by this setting. c_{eq} defines constraints for SRP force and torque applied on a spacecraft. In total, a successful optimal solution provides optimal attitude and joint angles that satisfy arbitrary target SRP force and torque while achieving (neutrally) stable attitude motion. We solved the optimization problem defined in Eq. (18) by using `fmincon`, the constrained optimization solver in MATLAB. The algorithm of the solver is set to be the interior point method [32].

The target F_{targ} and T_{targ} can be arbitrary values as far as their magnitudes are within the range of available SRP force and torque. However, $T_{\text{targ}} = [0, 0, 0]^T$ is practically used in most cases because it generates (neutrally) stable equilibrium attitude satisfying arbitrary target SRP force, which is useful for orbit control. Therefore, we assume $T_{\text{targ}} = [0, 0, 0]^T$ in the following sections.

In this paper, initial guess of ϕ and θ are provided in the following procedure. First, the initial guess of joint configuration, θ_0 , is provided as the body configuration exhibits an "umbrella-like" shape against the sun; joints are folded such that the CoM of the body component moves opposite to the s direction. It has been pointed out that this umbrella-like body configuration improves stability of attitude oscillation under SRP torque field [33]. Next, the initial guess of Euler angles, ϕ_0 is provided as a normal vector of the body-0 points opposite to the direction of target SRP force. This initial guess is expected to make a direction of total SRP force be close to that of the target SRP force. Roll angle around the normal vector is not uniquely determined with this initial guess, and therefore, we adopts trial-and-error search; the roll angle from 0 to 2π is tested in a certain interval until the solver returns a successful (local) optimal solution.

3.2 Momentum damping control with joint actuation

As Chujo pointed out [22], the optimal solution obtained in Section 3.1 cannot stabilize rotation around the sun-pointing vector s because this rotation does not affect SRP torque expressed in body fixed frame. Therefore, minute residual angular velocity or angular acceleration around the vector s are never decelerated and generates attitude drift from the desired attitude. Chujo proposed damping control using reaction wheels, but this paper proposes damping control only with joint angle actuation. To construct this control law, the attitude equation of motion is extended into attitude-joint coupled equation as it also includes the counter rotation of attitude during joint actuation.

In the following formulations, the superscript $(\cdot)^I$ such as T^I and h_c^I indicates vector components expressed in inertial frame. Equation of motion that includes attitude reaction during joint actuation is expressed as follows using Eq. (5):

$$\begin{aligned}
T^I &= \frac{dh_c^I}{dt} \\
\leftrightarrow C^T T &= \frac{d}{dt}(C^T h_c) = \frac{d}{dt}(C^T M_{\omega\omega}\omega + C^T M_{\omega\theta}\dot{\theta}) \\
&= C^T \left\{ \omega^\times M_{\omega\omega}\omega + \left(\frac{\partial M_{\omega\omega}}{\partial \theta} \dot{\theta} \right) \omega + M_{\omega\omega}\dot{\omega} + \omega^\times M_{\omega\theta}\dot{\theta} + \left(\frac{\partial M_{\omega\theta}}{\partial \theta} \dot{\theta} \right) \dot{\theta} + M_{\omega\theta}\ddot{\theta} \right\} \\
&\simeq C^T (M_{\omega\omega}\dot{\omega} + M_{\omega\theta}\ddot{\theta}) \\
\leftrightarrow T &= M_{\omega\omega}\dot{\omega} + M_{\omega\theta}\ddot{\theta} \simeq M_{\omega\omega} C_\phi^{-1} \ddot{\phi} + M_{\omega\theta}\ddot{\theta}
\end{aligned} \tag{20}$$

where C is a direction cosine matrix of body frame with respect to inertial frame. Here we assumed $|\omega|, |\dot{\theta}| \ll 1$ and second order terms of them are ignored. Now, this equation is linearized around equilibrium state to construct the control law. The equilibrium states \tilde{T} , $\tilde{\phi}$, and $\tilde{\theta}$ and difference from the equilibrium states δT , $\delta\phi$, and $\delta\theta$ satisfy the following equations:

$$T = \tilde{T} + \delta T = \delta T, \quad \phi = \tilde{\phi} + \delta\phi, \quad \theta = \tilde{\theta} + \delta\theta \tag{21}$$

δT can be expressed as follows according to Eq. (9):

$$\delta T(\delta\phi, \delta\theta) = \frac{\partial T}{\partial \phi}(\tilde{\phi}, \tilde{\theta})\delta\phi + \frac{\partial T}{\partial \theta}(\tilde{\phi}, \tilde{\theta})\delta\theta \tag{22}$$

Thus, the equation of motion can be linearized around equilibrium state as follows:

$$\begin{aligned} \delta T &= \frac{\partial T}{\partial \phi} \delta \phi + \frac{\partial T}{\partial \theta} \delta \theta = M_{\omega\omega} C_\phi^{-1} \delta \ddot{\phi} + M_{\omega\theta} \delta \ddot{\theta} \\ \Leftrightarrow \delta \ddot{\phi} &= C_\phi M_{\omega\omega}^{-1} \frac{\partial T}{\partial \phi} \delta \phi + C_\phi M_{\omega\omega}^{-1} \frac{\partial T}{\partial \theta} \delta \theta - C_\phi M_{\omega\omega}^{-1} M_{\omega\theta} \delta \ddot{\theta} \end{aligned} \quad (23)$$

Finally, a linearized equation of motion of the attitude-joint coupled motion is provided as follows:

$$\begin{aligned} \frac{d}{dt} \begin{bmatrix} \delta \phi \\ \delta \theta \\ \delta \dot{\phi} \\ \delta \dot{\theta} \end{bmatrix} &= \begin{bmatrix} O_{3 \times 3} & O_{3 \times m} & U_{3 \times 3} & O_{3 \times m} \\ O_{m \times 3} & O_{m \times m} & O_{m \times 3} & U_{m \times m} \\ C_\phi M_{\omega\omega}^{-1} \frac{\partial T}{\partial \phi} & C_\phi M_{\omega\omega}^{-1} \frac{\partial T}{\partial \theta} & O_{3 \times 3} & O_{3 \times m} \\ O_{m \times 3} & O_{m \times m} & O_{m \times 3} & O_{m \times m} \end{bmatrix} \begin{bmatrix} \delta \phi \\ \delta \theta \\ \delta \dot{\phi} \\ \delta \dot{\theta} \end{bmatrix} + \begin{bmatrix} O_{3 \times m} \\ O_{m \times m} \\ -C_\phi M_{\omega\omega}^{-1} M_{\omega\theta} \\ U_{m \times m} \end{bmatrix} \delta \ddot{\theta} \\ \Leftrightarrow \frac{dx}{dt} &= Ax + Bu \end{aligned} \quad (24)$$

where

$$A = \begin{bmatrix} O_{3 \times 3} & O_{3 \times m} & U_{3 \times 3} & O_{3 \times m} \\ O_{m \times 3} & O_{m \times m} & O_{m \times 3} & U_{m \times m} \\ C_\phi M_{\omega\omega}^{-1} \frac{\partial T}{\partial \phi} & C_\phi M_{\omega\omega}^{-1} \frac{\partial T}{\partial \theta} & O_{3 \times 3} & O_{3 \times m} \\ O_{m \times 3} & O_{m \times m} & O_{m \times 3} & O_{m \times m} \end{bmatrix}, \quad B = \begin{bmatrix} O_{3 \times m} \\ O_{m \times m} \\ -C_\phi M_{\omega\omega}^{-1} M_{\omega\theta} \\ U_{m \times m} \end{bmatrix} \quad (25)$$

U and O are identity and zero matrices respectively, and the subscript $()_{m \times n}$ denotes that the dimension of the matrix is $m \times n$. In this paper, the control input u is set to be angular acceleration of joints, although the actual motor does not necessarily control angular acceleration. To stabilize this system, we adopt the linear-quadratic regulator (LQR). The LQR feedback was proposed by Kalman [34], in which an objective function f is provided as quadratics of state and input for linearized system as follows:

$$f = \int_0^\infty (x^\top Q x + u^\top R u) dt \quad (26)$$

Then, the optimal feedback control law is provided as follows:

$$u = -R^{-1} B^\top X x \quad (27)$$

where X is a solution of Riccati equation $XA + A^\top X - XBR^{-1}B^\top X + Q = 0$. The weight matrices Q and R are provided as follows:

$$\begin{aligned} Q &= \begin{bmatrix} Q_{11} & O & O & O \\ & Q_{22} & O & O \\ & O & Q_{33} & O \\ & O & O & Q_{44} \end{bmatrix}, \quad R = \begin{bmatrix} |\delta \ddot{\theta}_1|^{-2} & O & O \\ & \ddots & \\ O & & |\delta \ddot{\theta}_m|^{-2} \end{bmatrix} \\ Q_{11} &= \begin{bmatrix} |\delta \phi_1|^{-2} & O & O \\ O & |\delta \phi_2|^{-2} & O \\ O & O & |\delta \phi_3|^{-2} \end{bmatrix}, \quad Q_{22} = \begin{bmatrix} |\delta \theta_1|^{-2} & O & O \\ O & \ddots & \\ O & & |\delta \theta_m|^{-2} \end{bmatrix} \\ Q_{33} &= \begin{bmatrix} |\delta \dot{\phi}_1|^{-2} & O & O \\ O & |\delta \dot{\phi}_2|^{-2} & O \\ O & O & |\delta \dot{\phi}_3|^{-2} \end{bmatrix}, \quad Q_{44} = \begin{bmatrix} |\delta \dot{\theta}_1|^{-2} & O & O \\ O & \ddots & \\ O & & |\delta \dot{\theta}_m|^{-2} \end{bmatrix} \end{aligned} \quad (28)$$

where the order of magnitude of each state component is provided as follows:

$$\begin{aligned} |\delta \phi_i| &\simeq \frac{\pi}{180}, \quad |\delta \theta_j| \simeq \frac{\pi}{180} \quad (i = 1, 2, 3, j = 1, \dots, m) \\ |\delta \dot{\phi}_i| &\simeq \omega_n |\delta \phi_i|, \quad |\delta \dot{\theta}_j| \simeq \omega_n |\delta \theta_j|, \quad |\delta \ddot{\theta}_j| \simeq \omega_n^2 |\delta \theta_j| \end{aligned} \quad (29)$$

The natural angular frequency ω_n can be estimated by frequency of uncontrolled attitude motion under SRP, hence $\omega_n = \left\| \text{Im} \left(\sqrt{\Lambda} \right) \right\|_\infty$.

LQR feedback control is a typical example to stabilize the system, but it is not the unique solution. Application of other effective control laws is in the scope of future works.

4 Numerical simulations

This section provides a numerical simulation to validate the proposed joint optimization and feedback control law to stabilize the attitude motion. As described in Section 3, our proposed methods are effective for a transformable spacecraft that has front faces that can dominantly receive SRP on each body. A mathematical model of a transformable spacecraft used in this paper is shown in Fig. 4. This model consists of nine square flat panels connected with actuatable

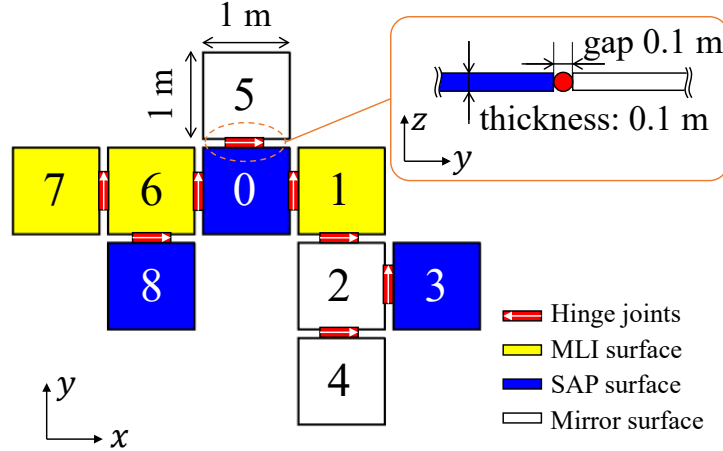


Figure 4: Model of a transformable solar sail used in the simulation

hinge joints. All panels has identical dimensions; $1\text{ m} \times 1\text{ m} \times 0.1\text{ m}$ size and 10 kg mass with homogeneous density. The number of actuatable joints are determined to ensure sufficient control degree of freedom to obtain successful solutions. The configuration shown in this figure exhibits the joint angles are all zero, and local coordinates coincide with the body-fixed coordinate attached to the body 0 that is shown at the left-bottom part of this figure. The positive direction of joint axis is shown in a white arrow on the hinge joint in Fig. 4. The gaps between panels are same as thickness of a panel (0.1 m), and the axis of joints are located at the middle of the gap. Moreover, the panels and its optical properties are randomly distributed to demonstrate that our proposed method is valid for an arbitrary transformable spacecraft. Three surface materials, multi-layer insulation (MLI), solar array panel (SAP) and ideally reflective mirror are prepared as representative surface materials. Surface materials of bodies are indicated by colors in Fig. 4 where the color labels are described at the right-bottom corner. The values of optical properties are listed in Table 1. As is

Table 1: List of optical properties

Material	C_{spe}	C_{dif}	C_{abs}
MLI	0.375	0.255	0.370
SAP	0.086	0.060	0.854
Mirror	1.0	0.0	0.0

explained in Section 2.2, SRP is exerted on all flat faces directed toward the sun. The control law is constructed so that only Jacobians of front faces are taken into account. The following simulation confirms the control law is valid for this panel-based transformable spacecraft.

4.1 SRP-based joint angle optimization

First, the SRP-based joint angle optimization is carried out. Target SRP force and torque are set as $F_{\text{targ}}^{\text{I}} = 10^{-4} \times [-0.0868, -0.0434, -0.4340]^{\text{T}}$ (N) and $T_{\text{targ}} = [0, 0, 0]^{\text{T}}$ (N·m) respectively. Notice that components of the target force is expressed in inertial frame. Distance from the sun is set as 1.01 AU , which corresponds to the distance between the sun and the Sun-Earth 2nd Lagrange point. As mentioned in Section 2.3, we use 2-1-3 Euler angles for numerical integration. Initial guess of attitude ϕ and joint angles θ are respectively provided as $\phi_0 = [11.31, -5.60, 0.00]^{\text{T}}$ (deg) and $\theta_0 = [30, 0, 0, 0, -30, -30, 0, 0]^{\text{T}}$ (deg). The initial configuration is illustrated in Fig. 5. In this condition, the optimal attitude and joint configuration obtained by the solver are $\phi = [27.72, -22.38, -10.23]^{\text{T}}$ (deg) and

$\theta = [11.87, 28.21, -13.14, -3.86, 2.79, -35.39, -12.89, 6.21]^T$ (deg) respectively. The result is illustrated in Fig. 6.

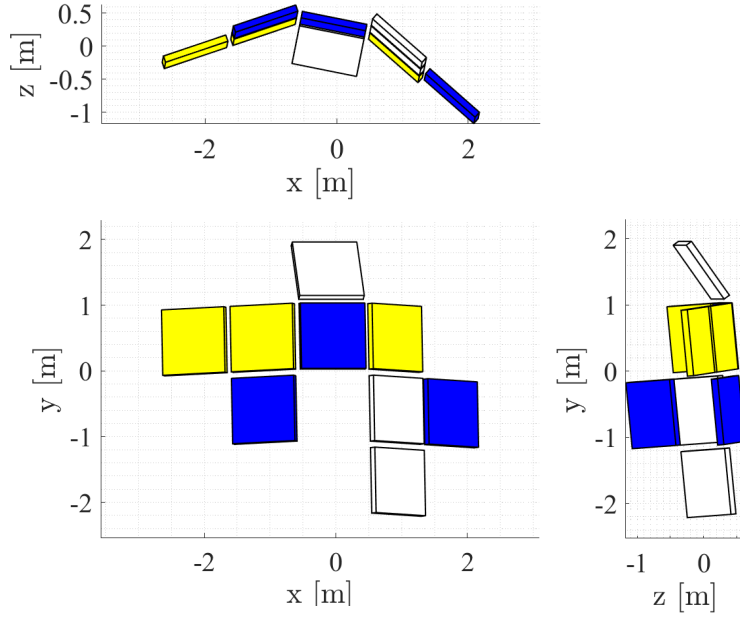


Figure 5: Initial guess of SRP-based joint angle optimization

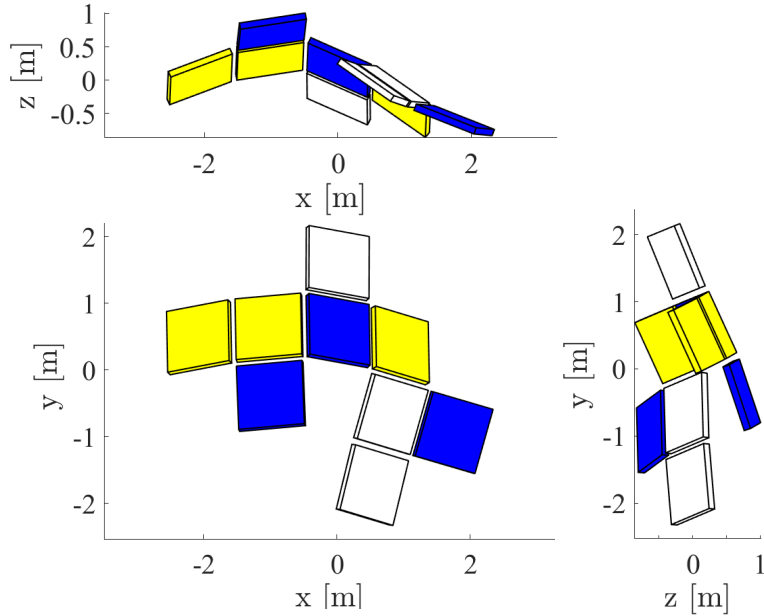


Figure 6: Result of SRP-based joint angle optimization

4.2 Joint-driven attitude stabilization

Now, the stability of the obtained equilibrium state is examined with a simulation. First, the stability without feedback control is examined. Initial errors of attitude and angular velocity from the equilibrium state are set as $\delta\phi_0 = [0.819, 0.567, 0.088]^T$ (deg) and $\omega_0 = [10^{-3} \ 10^{-3} \ 10^{-3}]^T$ (deg/s). $\delta\phi_0$ was randomly sampled as the

magnitude of the error becomes 1 degree. The numerical integration is carried out with ode45 solver in MATLAB with absolute and relative tolerance 10^{-5} and 10^{-6} respectively. Figure 7 and 8 show the time histories of Euler angles, angular velocities, and SRP force and torque. Without momentum damping control, the attitude oscillation around the

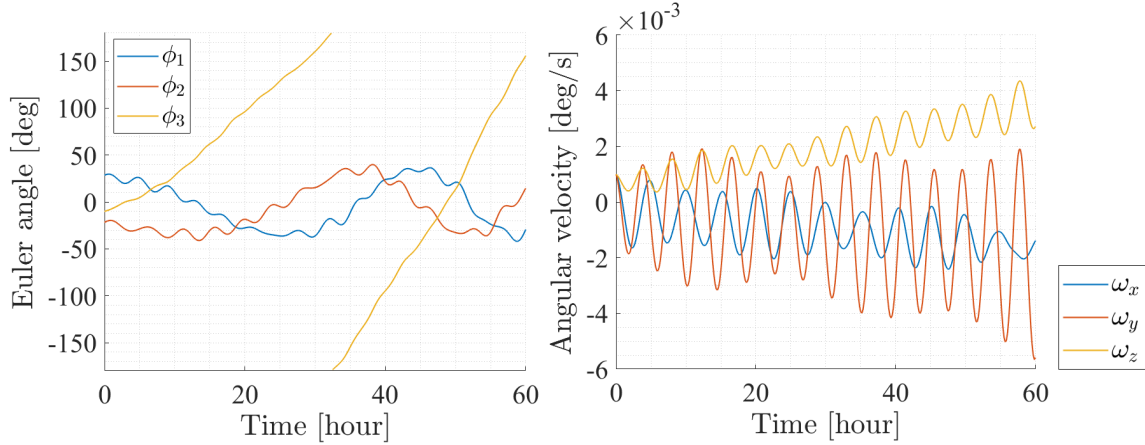


Figure 7: Time history of Euler angles and angular velocity without momentum damping control

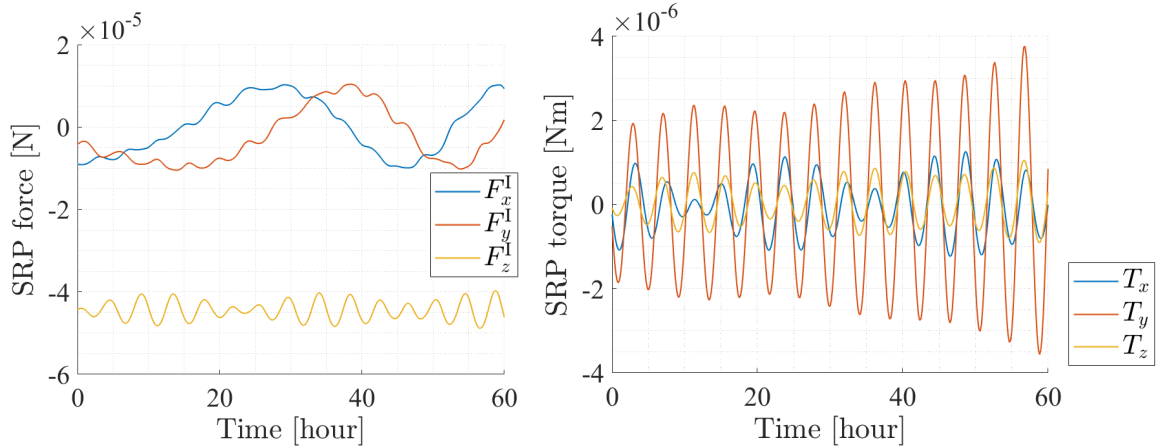


Figure 8: Time history of SRP force and Torque without momentum damping control

equilibrium point is never suppressed and gradually drifted from the equilibrium attitude. Thus, the result shows the necessity of momentum damping control to maintain the optimal configuration.

Next, momentum damping control is carried out for the system to stabilize the attitude motion. The same initial conditions, $\delta\phi_0 = [0.819, 0.567, 0.088]^T$ (deg) and $\omega_0 = [10^{-3} 10^{-3} 10^{-3}]^T$ (deg/s) are also used for this simulation. The natural frequency of the attitude oscillation becomes $\omega_n = 4.23 \times 10^{-4}$ (1/s) in this case, and this value is reflected to the weight matrices Q , R of the LQR feedback. Figure 9–11 show the result of the simulation with the momentum damping control. Figure 10 is expressed as difference from the equilibrium joint angles. All the figures show that the initial error of the attitude and angular velocity are suppressed and the momentum damping is successfully completed while final values of attitude and joint configuration are converged to the target state obtained in Section 4.1. As a result, the transformable spacecraft can stably acquire the desired SRP acceleration without consuming any expendable propellant.

5 Conclusions

The present work contributed to enhancing orbit control capability of transformable spacecrafts. Though the transformable spacecrafts have high redundancy in control degree of freedom, its large number of control inputs imposed

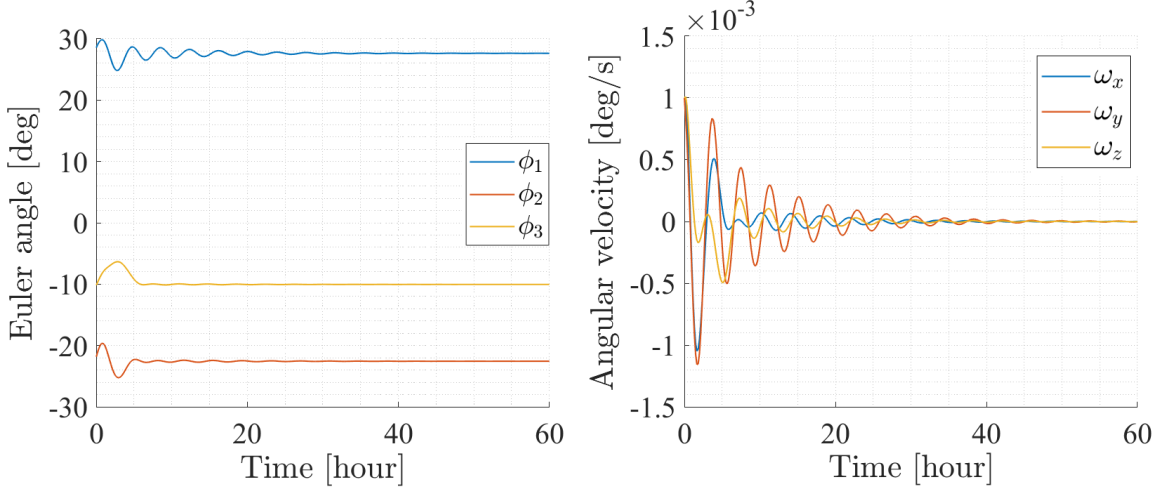


Figure 9: Time history of Euler angles and angular velocity

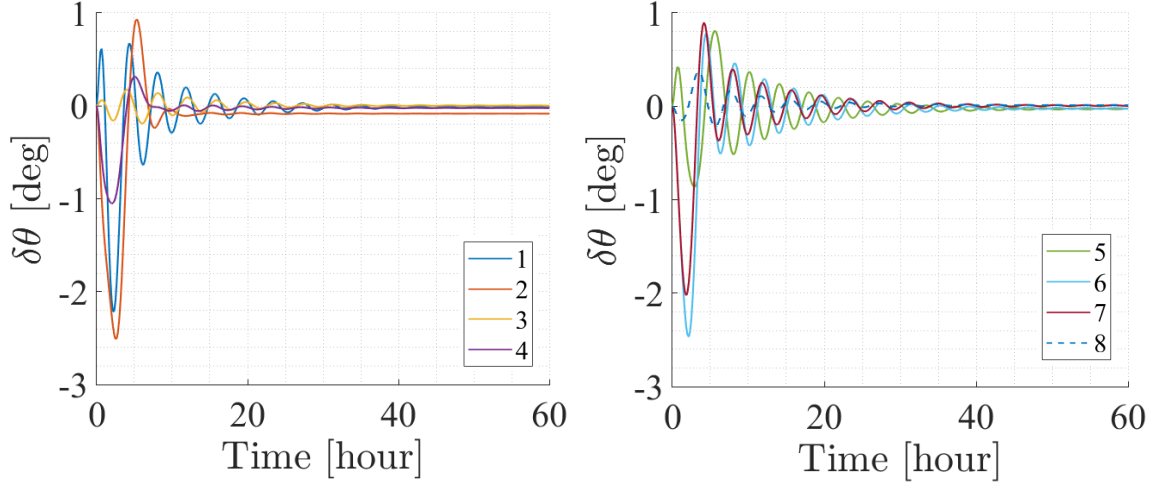


Figure 10: Time history of joint angle difference from the equilibrium configuration

difficulties in control in previous studies. This paper solved this problem with two novel proposed techniques. First, we proposed the optimization method to obtain attitude and joint configuration to satisfy arbitrary SRP force and torque while preventing divergence of attitude. Second, we proposed the momentum damping control formulated under attitude-joint coupled dynamics. What distinguishes these methods from other previous methods is that they are generally applicable to any transformable spacecraft that has front faces that can dominantly receive SRP on each body. Through the proposed methods, arbitrary transformable spacecrafts can acquire desired SRP acceleration without consuming any expendable propellant. These control methods are essential for zero-momentum transformable spacecrafts to accomplish desired orbit maneuver under solar radiation pressure.

Appendix A

Mathematical expressions in this appendix follow the formulations in Ref. [35]. The explicit expressions in Equation (1), which can be derived through the Kane method [30], are provided in the equations that follow. Note that f_X and f_X^\dagger are external and inertial force exerted on the CoM of body X respectively, whereas n_X and n_X^\dagger are external and inertial torque exerted on the body X respectively. n_{θ_i} is the actuation torque of the i -th hinge joint. Other characters

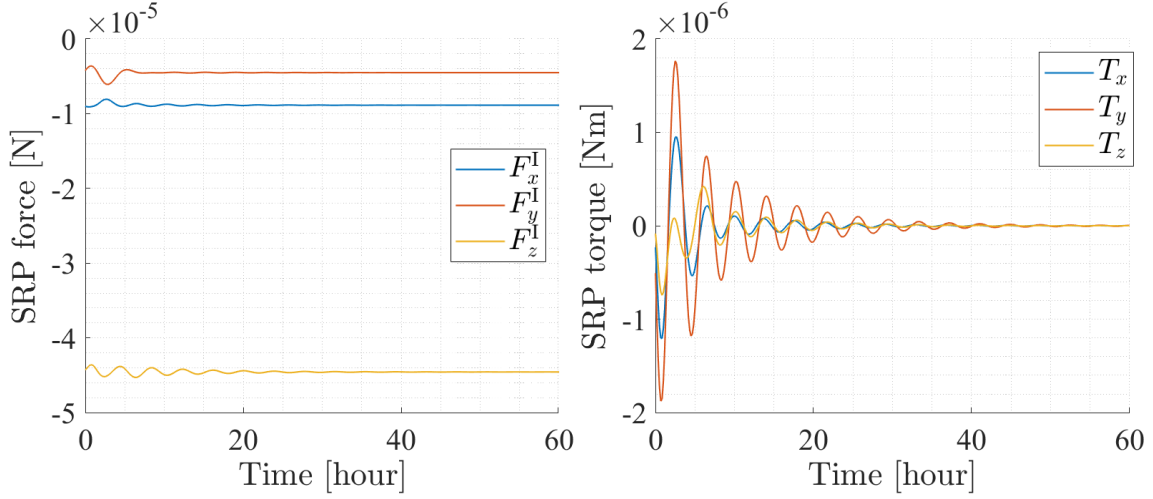


Figure 11: Time history of SRP force and Torque

can be interpreted with the nomenclature list at the beginning of this paper.

$$\begin{aligned}
M_{vv} &= m_c U \\
M_{\omega\omega} &= I_c \\
M_{\omega\theta,j} &= \left(I_{\hat{j}} - m_{\hat{j}} r_{\hat{j}c}^{\times} r_{\hat{j}h_j}^{\times} \right)^{\top} \lambda_j \\
M_{\theta\omega,i} &= \lambda_i^{\top} \left(I_{\hat{i}} - m_{\hat{i}} r_{\hat{i}c}^{\times} r_{\hat{i}h_i}^{\times} \right) \\
M_{\theta\theta,ij} &= M_{\theta\theta,ij}^* + \frac{m_{\hat{i}} m_{\hat{j}}}{m_c} \lambda_i^{\top} \left(r_{\hat{i}h_i}^{\times} r_{\hat{j}h_j}^{\times} \right)^{\top} \lambda_j \\
M_{\theta\theta,ij}^* &= \begin{cases} \lambda_i^{\top} \left(I_{\hat{j}} - m_{\hat{j}} r_{\hat{j}h_i}^{\times} r_{\hat{j}h_j}^{\times} \right)^{\top} \lambda_j & (j \in \hat{i}) \\ \lambda_i^{\top} \left(I_{\hat{i}} + m_{\hat{i}} r_{\hat{i}h_i}^{\times} r_{\hat{i}h_j}^{\times} \right)^{\top} \lambda_j & (i \in \hat{j}) \\ 0 & (i \notin \hat{j} \cap j \notin \hat{i}) \end{cases} \\
M_{v\omega} &= M_{v\theta} = M_{\omega v} = M_{\theta v} = O \quad (\text{Zero matrix})
\end{aligned} \tag{30}$$

$$\begin{aligned}
d_v &= m_c \omega^{\times} \dot{R}_c \\
d_{\omega} &= \sum_k \left\{ (R_k - R_c)^{\times} f_k^{\dagger} + n_k^{\dagger} \right\} \\
d_{\theta,i} &= \lambda_i^{\top} \left[\sum_{k \in \hat{i}} \left\{ (R_k - R_{h_i})^{\times} f_k^{\dagger} + n_k^{\dagger} \right\} - m_{\hat{i}} r_{\hat{i}h_i}^{\times} \omega^{\times} \dot{R}_c \right]
\end{aligned} \tag{31}$$

$$\begin{aligned}
\tau_v &= f_c \\
\tau_{\omega} &= \sum_k \left\{ (R_k - R_c)^{\times} f_k + n_k \right\} \\
\tau_{\theta,i} &= \lambda_i^{\top} \left[\sum_{k \in \hat{i}} \left\{ (R_k - R_{h_i})^{\times} f_k + n_k \right\} - \sum_k \frac{m_{\hat{i}}}{m_c} \left(r_{\hat{i}h_i}^{\times} f_k \right) \right] + n_{\theta_i}
\end{aligned} \tag{32}$$

where $M_{\omega\theta,j}$ is the j -th column of $M_{\omega\theta}$, $M_{\theta\omega,i}$ is the i -th row of $M_{\theta\omega}$, $d_{\theta,i}$ is the i -th component of d_{θ} , and $\tau_{\theta,i}$ is the i -th component of τ_{θ} .

Acknowledgements

The present study was supported by Advisory Committee for Space Engineering in Japan as a strategic research working group. The authors are grateful to the members of the Transformer working group that greatly enhanced the value of the present study through thorough and patient discussions.

Declaration of competing interest

The authors declare that they have no known competing financial interests or personal relationships that could have appeared to influence the work reported in this paper.

References

- [1] C Sauer Jr. “Optimum solar-sail interplanetary trajectories”. In: *Astrodynamics Conference*. 1976, p. 792.
- [2] M Leipold and O Wagner. “Solar Photonic Assist Trajectory Design for Solar Sail Missions to the Outer Solar System and Beyond”. In: *Spaceflight Dynamics 1998* 100 (1998).
- [3] Colin R McInnes et al. “Solar sail parking in restricted three-body systems”. In: *Journal of Guidance, Control, and Dynamics* 17.2 (1994), pp. 399–406.
- [4] H Baoyin and CR. McInnes. “Solar sail halo orbits at the Sun–Earth artificial L_1 point”. In: *Celestial Mechanics and Dynamical Astronomy* 94.2 (2006), pp. 155–171.
- [5] Go Ono et al. “Generalized attitude model for momentum-biased solar sail spacecraft”. In: *Journal of Guidance, Control, and Dynamics* 39.7 (2016), pp. 1491–1500.
- [6] Yuichi Tsuda, Go Ono, and Yuya Mimasu. “Classification of solar sail attitude dynamics with and without angular momentum”. In: *Astrodynamics* 3.3 (2019), pp. 207–216. DOI: 10.1007/s42064-018-0045-6.
- [7] Jiafu Liu et al. “Dynamic modeling and analysis of a flexible sailcraft”. In: *Advances in Space Research* 56.4 (2015), pp. 693–713.
- [8] Jiafu Liu, Liqun Chen, and Naigang Cui. “Solar sail chaotic pitch dynamics and its control in Earth orbits”. In: *Nonlinear Dynamics* 90 (2017), pp. 1755–1770.
- [9] Osamu Mori et al. “First solar power sail demonstration by IKAROS”. In: *Transactions of the Japan Society for Aeronautical and Space Sciences, Aerospace Technology Japan* 8.ists27 (2010), To_4_25–To_4_31.
- [10] Yuichi Tsuda et al. “Flight status of IKAROS deep space solar sail demonstrator”. In: *Acta astronautica* 69.9-10 (2011), pp. 833–840.
- [11] David A Spencer et al. “The LightSail 2 solar sailing technology demonstration”. In: *Advances in Space Research* 67.9 (2021), pp. 2878–2889.
- [12] Yuki Takao et al. “Active shape control of spinning membrane space structures and its application to solar sailing”. In: *Transactions of the Japan Society for Aeronautical and Space Sciences* 61.3 (2018), pp. 119–131.
- [13] Yuki Takao, Osamu Mori, and Jun’ichiro Kawaguchi. “Optimal interplanetary trajectories for spinning solar sails under sail-shape control”. In: *Journal of Guidance, Control, and Dynamics* 42.11 (2019), pp. 2541–2549.
- [14] Yuki Takao, Osamu Mori, and Jun’ichiro Kawaguchi. “Self-excited oscillation of spinning solar sails utilizing solar radiation pressure”. In: *Astrodynamics* 4.3 (2020), pp. 177–192.
- [15] Yoshihiko Nakamura and Ranjan Mukherjee. “Nonholonomic path planning of space robots via bi-directional approach”. In: *Proceedings of IEEE International Conference on Robotics and Automation*. IEEE. 1990, pp. 1764–1769.
- [16] Evangelos G Papadopoulos. “Path Planning For Space Manipulators Exhibiting Nonholonomic Behavior.” In: *IROS*. 1992, pp. 669–675.
- [17] Richard M Murray and S Shankar Sastry. “Nonholonomic motion planning: Steering using sinusoids”. In: *IEEE transactions on Automatic Control* 38.5 (1993), pp. 700–716.
- [18] Kaoru Ohashi, Toshihiro Chujo, and Junichiro Kawaguchi. “Optimal motion planning in attitude maneuver using non-holonomic turns for a transformable spacecraft”. In: *AAS/AIAA Astrodynamics Specialist Conference, 2018*. Univelt Inc. 2018, pp. 2735–2745.
- [19] Shengping Gong, Haoran Gong, and Peng Shi. “Shape-Based Approach to Attitude Motion Planning of Reconfigurable Spacecraft”. In: *Advances in Space Research* (2022).
- [20] Yuki KUBO and Junichiro KAWAGUCHI. “Approximate Analytical Solution for Attitude Motion of a Free-flying Space Robot and Analysis of Its Nonholonomic Properties”. In: *TRANSACTIONS OF THE JAPAN SOCIETY FOR AERONAUTICAL AND SPACE SCIENCES, AEROSPACE TECHNOLOGY JAPAN* 20 (2022), pp. 35–40.

-
- [21] Yuki Kubo and Junichiro Kawaguchi. “Nonholonomic Reorientation of Free-Flying Space Robots Using Parallelogram Actuation in Joint Space”. In: *Journal of Guidance, Control, and Dynamics* (2022), pp. 1–11.
- [22] Toshihiro Chujo. “Propellant-free attitude control of solar sails with variable-shape mechanisms”. In: *Acta Astronautica* 193 (2022), pp. 182–196.
- [23] Arya Abrishami and Shengping Gong. “Optimized control allocation of an articulated overactuated solar sail”. In: *Journal of Guidance, Control, and Dynamics* 43.12 (2020), pp. 2321–2332.
- [24] Haoran Gong, Shengping Gong, and Dali Liu. “Attitude dynamics and control of solar sail with multibody structure”. In: *Advances in Space Research* 69.1 (2022), pp. 609–619.
- [25] Yuki Kubo et al. “Preliminary study on system and mission sequence design for Transformer mission”. In: *73rd International Astronautical Congress*. International Astronautical Federation, 2022.
- [26] Kiyona Miyamoto et al. “On-Orbit Verification of Attitude Dynamics of Satellites with Variable Shape Mechanisms using Atmospheric Drag Torque and Gravity Gradient Torque”. In: *AIAA SCITECH 2023 Forum*. 2023, p. 0933.
- [27] Toshihiro Chujo et al. “Orbit-Attitude Integrated Control on Small-Amplitude Periodic Orbit around Sun-Earth L2 in Transformer Mission”. In: *73rd International Astronautical Congress*. International Astronautical Federation, 2022.
- [28] Yuki Kubo. “Simultaneous Body Reconfiguration and Nonholonomic Attitude Reorientation of Free-flying Space Robots”. PhD thesis. The University of Tokyo, 2022.
- [29] Thomas R Kane and David A Levinson. “The use of Kane’s dynamical equations in robotics”. In: *The International Journal of Robotics Research* 2.3 (1983), pp. 3–21. DOI: 10.1177/027836498300200301.
- [30] Thomas R Kane and David A Levinson. *Dynamics, theory and applications*. McGraw Hill, 1985.
- [31] Colin R McInnes. *Solar sailing: technology, dynamics and mission applications*. Springer Science & Business Media, 2004.
- [32] Richard H Byrd, Mary E Hribar, and Jorge Nocedal. “An interior point algorithm for large-scale nonlinear programming”. In: *SIAM Journal on Optimization* 9.4 (1999), pp. 877–900.
- [33] Yuki Kubo, Toshihiro Chujo, and Junichiro Kawaguchi. “Propellant-Free Station Keeping around Sun-Earth L2 Using Solar Radiation Pressure for a Transformable Spacecraft”. In: *32nd International Symposium on Space Technology and Science*. JSASS, 2019.
- [34] Rudolf Emil Kalman et al. “Contributions to the theory of optimal control”. In: *Bol. soc. mat. mexicana* 5.2 (1960), pp. 102–119.
- [35] Katsuhiko Yamada. “Handbook of Spacecraft Dynamics and Control: From Fundamental Theory to Applied Technologies (Japanese)”. In: ed. by Attitude Control Research Committee. Baifukan, 2007. Chap. 4.3, Appendix A.